# Supplementary Information

Benedict Winchester[1,2], Gan Huang[1,3], Hamish Beath[4], Philip Sandwell[2,4], Jiajun Cen[5,6], Jenny Nelson[4] and Christos N. Markides[1*]

[1*]Clean Energy Processes (CEP) Laboratory, Department of Chemical Engineering, Imperial College London, London, SW7 2AZ, United Kingdom.
[2]Grantham Institute – Climate Change and the Environment, Imperial College London, London, SW7 2AZ, United Kingdom.
[3]Institute of Microstructure Technology, Karlsruhe Institute of Technology, Karlsruhe, 76133, Germany.
[4]Department of Physics, Imperial College London, London, SW7 2AZ, United Kingdom.
[5]Department of Chemical Engineering, Imperial College London, London, SW7 2AZ, United Kingdom.
[6]Desolenator B.V., Ankerkade 141, 6222 NL, Maastricht, The Netherlands.

*Corresponding author(s). E-mail(s): c.markides@imperial.ac.uk;

## 1 Component degradation

We degrade the electrical performance of the PV and PV-T collectors and the installed batteries over their lifetime using an average degradation rate of 1.1 %/year in efficiency for PV modules [1] and manufacturer-specific degradation values for the batteries considered.

### 1.1 Collector degradation

The annual PV degradation rate is expressed as a fraction of its present-day performance per year. Hence, to determine the performance of the PV collectors on an average day, we consider the total power that they can provide over their lifetime by integrating their degradation curve over each of the years for which they provide electricity to the system:

$$\overline{P}_{\mathrm{pv}} = \left(1 - \overline{d}_{\mathrm{pv}}\right) P_{\mathrm{pv,undeg}} = \int_0^N \left(1 - d_{\mathrm{pv}}\right)^k \,\mathrm{dk} = \frac{\left(1 - d_{\mathrm{pv}}\right)^N - 1}{\log\left(1 - d_{\mathrm{pv}}\right)}, \quad (1)$$

where $\overline{P}_{\mathrm{pv}}$ is the power outputted by the PV/PV-T collectors over an average day, $\overline{d}_{\mathrm{pv}}$ the average electrical degradation experienced by the panels, $P_{\mathrm{pv,undeg}}$ the power outputted by the PV/PV-T collectors over an average day with no degradation effects considered, $N$ the lifetime of the system in years and $d_{\mathrm{pv}}$ the annual degradation of the PV/PV-T modules taken from literature.

Little literature exists on the degradation of the electrical performance of PV-T collectors over their lifetime as they will, in general, operate at a different range of temperatures to standalone PV panels. Various effects, such the peak day- and night-time temperatures that the panels are exposed to, and the average module temperature over the collector lifetime, are little understood. As such, we take the electrical degradation rate of the PV-T collectors considered are taken to be the same as those for the PV modules.

## 1.2 Battery degradation

The degradation of the batteries considered is based on the total power that has passed through them over the course of the lifetime of the plant. As we are considering the average performance of the plant, the same load profile is assumed for each day of the simulation. Hence, the degradation is given by

$$d_{\mathrm{batt}} = \frac{Q_{\mathrm{c}} N_{\mathrm{c}}}{Q_{\mathrm{max}} N_{\mathrm{L}}} d_{\mathrm{L}}, \quad (2)$$

where $d_{\mathrm{batt}}$ is the fractional degradation of the batteries at the end of the simulation period or when replaced, $Q_{\mathrm{c}}$ the charge which has passed through the batteries over the course of a day, $N_{\mathrm{c}}$ the number of cycles that have been performed over the lifetime of the plant, $Q_{\mathrm{max}}$ the maximum charge which can be stored in the batteries, $N_{\mathrm{L}}$ the number of full cycles which can be performed before the batteries are fully degraded such that $Q_{\mathrm{max}} N_{\mathrm{L}}$ gives the amount of charge which will have passed through the batteries when fully degraded, and $d_{\mathrm{L}}$ the fractional lifetime loss in the capacity of the batteries.

The average degradation rate of the batteries, $\overline{d}_{\mathrm{batt}}$, which we take to be a percentage drop in their capacity per year, is calculated as an average of the batteries which were fully exhausted and replaced during the lifetime of the plant, as well as those which remain at the end of the optimisation period. Hence, the average rate is taken as 50% for all replaced batteries combined with the average degradation of the batteries at the end of the lifetime:

$$\overline{d}_{\mathrm{batt}} = \frac{0.5\lfloor d_{\mathrm{batt}} \rfloor + 0.5\left(d_{\mathrm{batt}} \bmod 1\right)^2}{d_{\mathrm{batt}}}, \quad (3)$$

where $\lfloor d_{\text{batt}} \rfloor$ is the degradation of the batteries rounded down to the nearest integer, i.e., the number of replacements which occurred in the simulation, and $d_{\text{batt}} \bmod 1$ is the remainder when $d_{\text{batt}}$ is divided by one, i.e., the fractional degradation of the batteries that are most-recently installed.

This approach aims to capture the effect of the number of charge-discharge cycles on the health of the batteries. We neglect however the temperature-related effects as well as the impacts of deep discharges on the health of the batteries [2]. By averaging over the weather conditions, including the solar irradiance and ambient temperature, at each case-study location considered, we use degradation rates based on the average throughput of the batteries, i.e., for the average environmental conditions, at each location considered, and thus miss the impacts of temperature extremes [3]. Further, by considering the profile over an average day, we miss deeper discharges which occur when the solar resource is lower.

# 2 Lifetime-emissions analysis

To determine the system best able to provide clean water through desalination in line with the United Nations SDGs [4], it is necessary to quantify, not only the costs, but also the environmental impact of these systems. For their climate-change impact, we quantify this in terms of their embedded carbon dioxide equivalent ($CO_2$eq) emissions.

## 2.1 Embedded component emissions

Estimates for the embedded emissions arising from each of the components used are given in Table 1. For all the embedded-emission estimates, emissions associated with import and distribution have been neglected as manufacturing emissions dominate the embedded emissions [5–7]. As the emissions associated with the energy-generation system dominate those arising from MED desalination plants, with estimates between 91% and 80% for fossil-fuel driven [8] and partially-renewable systems [9] respectively, we consider only the embedded emissions associated with the energy-generation system. The embedded emissions in the manufacture of the plant are included as a fractional uncertainty, represented with errorbars, in the results presented.

For the m-Si PV module, we used the embedded emissions calculated by Michael et al. [10] for a 325 $\text{W}_\text{p}$ m-Si panel, whilst for the p-Si PV module, we used the value obtained by Lu et al. [12] for the specific emissions embedded in p-Si panels. For the ETCs considered, we adjusted estimates for the embedded carbon emissions calcualted by Henein et al. [11] with parameters, such as the number of evacuated tubes and the length of the collector, used to scale the analysis for the ETCs considered.

For the S-T FPCs and PV-T collectors considered, we adjusted estimates for the embedded carbon emissions calculated by Michael et al. [10], with the area of the collectors used to scale these values. Here, we have assumed that, as the embedded emissions of a flat-plate S-T or PV-T system scale with

**Table 1** Estimates of the embedded greenhouse-gas emissions associated with the various components installed in the system

| Component | Manufacturer | Model | Embedded emissions per component / kg $CO_2$eq/component |
|---|---|---|---|
| Solar-thermal collectors | Solar Technologie International GmbH | FKF 240 V CuCu | $199.3^1$ [10] |
| | solardirekt24 GmbH | Eurotherm Solar Pro 20 | $563.93^1$ [11] |
| | Augusta Solar | AS 100 DF | $219.73^1$ [11] |
| Photovoltaic-thermal collectors | Dualsun | (insulated) Spring 300M | $316.14^1$ [10] |
| | Dualsun | (insulated) Spring 400M | $362.74^1$ [10] |
| | Solimpeks | Powervolt | $264.90^1$ [10] |
| Photovoltaic panels | REC | 325 N-Peak Mono | 158.9 [10] |
| | Sharp | ND-AF 330 C | 154.68 [12] |
| Auxiliary heat pump | N/A | Ammonia-based | $174.8^2$ / $kWh_{th}$ [13] |
| Lithium-ion battery | Renogy | 12V 100Ah | 58.8 - 326 [14] |
| Heat-transfer fluid pump | Grundfos | CRNF 15-1 A-CA-A-E-HQQE | 145 [7] |
| Hot-water tank | Grant | HPMONO/IND150 | $230^3$ [15, 16] |
| Inverter | Solis | S5-GR1P6K 5G (6 $kW_p$) | $651.0^3$ [17] - 750 [18] |

[1]Values adapted based on the geometric properties of the collectors. See Section 2.1 for more information on these calculations.

[2]Specific emissions were used for the auxiliary heat pump installed. See Section 2.1 for more information.

[3]Emissions estimate based on interpolation from available data to extract an estimate for the component considered. See Section 2.1 for more information.

the overall area of the collectors installed, the embedded emissions of each individual collector thus scale with its absorber area.

The specific embedded emissions for the heat pump used in the model were taken from Moret 2017 [13]. For the specific emissions of the Li-Ion batteries used, Philippot et al. [14] estimated the emissions to be 123 kg $CO_2$eq/kWh$_{el}$. However, there remains uncertainty in the embedded emissions of Li-Ion batteries, partially due to variations in the carbon intensity of the electricity used at the production stage which can contribute up to 80% of the total embedded emissions associated with the battery [14]. As such, this value is likely to change significantly over time as national electricity grids decarbonise. Hence, we use a range of values for the embedded emissions, shown as an error bar, from 49 to 272 kg $CO_2$eq/kWh$_{el}$ [14, 19].

For the heat-transfer fluid pump installed, we took the specific emissions to be 3.54 kg $CO_2$eq/kg, estimated by Todde et al. [7], which was scaled to the heat-pump model considered based on the net weight of the water pump. For the hot-water buffer tank installed, we used an exponential fit to estimates provided by the Chartered Institution of Building Service Engineers [15] with the weight of the particular 150 litre hot-water tank used [16].

For the embedded emissions of the solar inverters installed, a power-law fit was fitted to estimates produced by Tschümperlin et al. [17], with the value for a 6 kW$_{el}$ inverter obtained from the fit. This formed a lower-bound estimate of the embedded emissions of 651.0 kg$CO_2$. Constantino et al. [18] estimated the embedded emissions for solar inverters to be 125 kg$CO_2$/kW$_p$ which we used to produce an upper-bound estimate of 750 kg $CO_2$ for the inverter used.

Because the majority of emissions embedded in components are due to their manufacturing [5, 6], as countries reduce the carbon intensity of their grids in line with the Paris Agreement [20], the embedded emissions associated with these components are likely to decrease. By making our model open-source [21], we enable manufacturers and stakeholders to undertake updated analyses as associated embedded emissions decrease.

## 2.2 Grid-electricity emissions

Emissions values for the energy sourced directly from the grid are given in Table 2. By averaging over the lifetime performance of the plant, seasonal variations in the carbon emissions associated with the grid are neglected, thus limiting the accuracy of the emissions calculations. However, the low renewable fractions across the case-study locations considered means that these seasonal fluctuations in the carbon intensity of the grid are likely to be minimal: renwable power generation met less than 1% of electricity demand in the UAE as of 2022 [22], 16% on Gran Canaria as of 2021 [23], and less than 8% on average throughout Mexico [22] in 2022.

For the carbon emissions associated with grid-sourced electricity in Mexico, state-level figures have been used [24, 25]. Whilst this disaggregation enables separate emission analyses for the Tijuana and La Paz case-study MED plants, by not using the most up-to-date country-level figures, recent reductions in the

**Table 2** Emissions intensity of energy sourced from the grid in each of the four case-study locations considered. Data for Aby Dhabi, UAE, and Gando, Gran Canaria, is from 2020. Data for Tijuana is taken from the 2014 Climate Action Plan for the state [24]. Data for La Paz is taken from the 2015 Climate Action Plan for the state [25].

| Location | Emissions / g $CO_2$eq/kWh$_{el}$ |
|---|---|
| Abu Dhabi, UAE | 461.85 [26, 27] |
| Gando, Gran Canaria | 576.54 [28] |
| Tijuana, Mexico | 310 [24] |
| La Paz, Mexico | 890 [25] |

carbon intensity of the grid have been neglected. However, as the modelling methodology employed here considers the plants over their lifetime, emission reductions of 14% since 2010 [29] are likely to be negligible compared with emission reductions over the lifetime of the plant needed to meet Mexico's Nationally-Determined Contributions in-line with the Paris Agreement [20].

As there is uncertainty around the rate at which the national grid networks will decarbonise, we take present-day values for both the embedded emissions in components and those arising from grid-sourced electricity. This will result in an over-estimation of the carbon intensity of both grid-driven RO as well as the embedded emissions in any components which are replaced over the lifetime of the plant, i.e., batteries for electrical storage and solar inverters. By making our model open-source, we enable stakeholders and future researchers to re-run out optimisations as up-to-date figures become available [21].

# 3 Sensitivity analysis results

Results of the sensitivity analyses around the cycle lifetime of the batteries installed and the lifetime of the solar inverters are presented here. These were carried out due to uncertainties surrounding these values [3, 30–33].

## 3.1 Inverter-lifetime sensitivity analysis

Results for the smallest-scale desalination plant considered [34] of the effect of changing the lifetime of the solar inverters installed on the grid-, solar- and storage-electricity fractions are shown in Figure 1. The results show that, for inverter lifetimes longer than 17 years, increasing the lifetime of the inverters installed had no further effect on the overall fractions of power installed in the system. This is due to the 30-year horizon considered meaning that systems where the inverters were replaced after 17 years of use are equivalent to those where the inverters were replaced after 29 years of use, i.e., one replacement of the inverters during the lifetime of the plant. This effect also accounts for the step-wise changes at 9-, 7-, 5-, 3- and 1-year lifetimes as the number of replacements changes when the lifetime is reduced beyond these points.

The data show that for Abu Dhabi in the UAE, Gando on Gran Canaria and La Paz in Tijuana, reducing the inverter lifetime resulted, with some fluctuations for Abu Dhabi, in a reduction in the solar-electricity fraction with

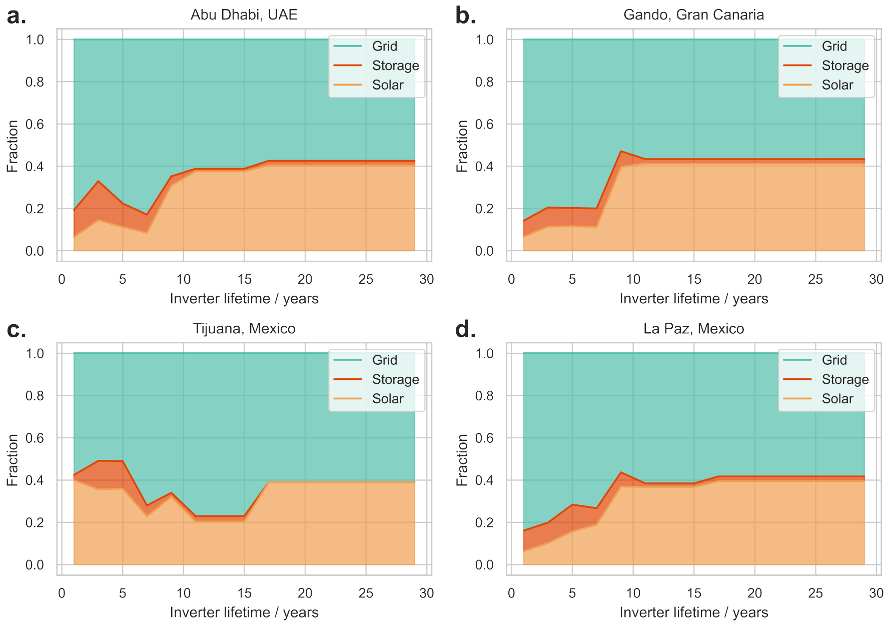


**Fig. 1 Sensitivity to inverter lifetime.** Line plot of the sources of electricity used to meet the MED desalination plant's electrical demands against the lifetime of the solar inverters installed for the smallest-scale desalination plant. Results are shown for a specific technology set: STI FPC S-T collectors, D.S. 400 PV-T collectors and Sharp p-Si PV panels. The battery cycle lifetime is fixed at 2000 cycles. Subfigures are for the four case-study locations: a. Abu Dhabi, UAE, b. Gando, Gran Canaria, c. Tijuana, Mexico and d. La Paz, Mexico. The data show that, for inverter lifetimes longer than 17 years, there is no change in the electricity fractions as the lifetime of the inverters changes. For inverter lifetimes shorter than 17 years, the optimum system displays volatility as well as a general trend that, with decreasing inverter lifetime, the storage and grid fractions increase whilst the solar fraction decreases. This trend is visible for Abu Dhabi, Gando and La Paz. For Tijuna, whilst there is a decrease in the solar fraction for short inverter lifetimes, there is also increased volatility in the storage, solar and grid fractions.

the storage- and grid-electricity fractions increasing. We attribute this to the reduced inverter lifetime resulting in systems that have a greater dependence on solar PV and PV-T collectors for electricity incurring greater costs over the lifetime of the system due to the increased costs associated with replacing the solar inverters more frequently. We attribute the fluctuations at short inverter lifetimes in part to the changing auxiliary-heating fraction and hence changes in the total electrical demand placed on the system which is not captured here.

The increase in the storage fraction for short inverter lifetimes suggests that electrical storage is utilised more during the morning and evening hours to meet demand as a more cost-effective means of providing electricity than potentially over-sizing a solar PV or PV-T system in order to meet these demands at the expense of dumping electricity during peak solar hours.

## 3.2 Battery lifetime sensitivity analysis

Results of the effect of changing the battery cycle lifetime on the grid-, solar- and storage-electricity fractions for the smallest-scale desalination plant considered are shown in Figure 2. The results show that, for Gando and La Paz, there is no discernible effect visible between battery lifetimes of 100 and 3000 cycles on the electricity fractions.

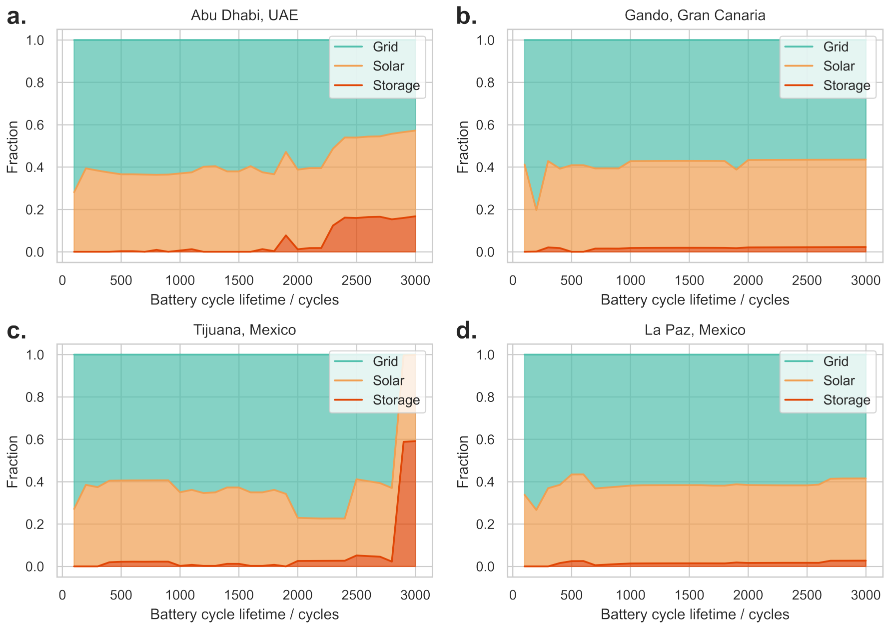


**Fig. 2 Sensitivity to battery cycle lifetime.** Line plot of the sources of electricity used to meet the MED desalination plant's electrical demands against the cycle lifetime of the lithium-ion batteries installed for the smallest-scale desalination plant. Results shown are for a specific technology set: STI FPC S-T collectors, D.S. 400 PV-T collectors and Sharp p-Si PV panels. The inverter lifetime is fixed at 15 years. Subfigures are for the four case-study locations: a. Abu Dhabi, UAE, b. Gando, Gran Canaria, c. Tijuana, Mexico and d. La Paz, Mexico. The data show that, for the most part, there is very little impact associated with changing the cycle lifetime of the batteries, with results for Gando on Gran Canaria and La Paz in Mexico being indistinguishable from fluctuations resulting from inherent randomness in the optimisation process. For Abu Dhabi in the UAE and Tijuana in Mexico, the results show distinct step changes where the battery cycle lifetime passes a threshold, around 2,300 cycles and 2,900 cycles for Abu Dhabi and Tijuana respectively, beyond which the storage fraction significantly increases.

For Abu Dhabi and Tijuana, the data in Figure 2 exhibit step changes in the storage-electricity fraction of 20.1% and 59.2% at around 2,300 cycles and 2,900 cycles for Abu Dhabi and Tijuana respectively. These step changes are likely due to a threshold being passed beyond which electrical storage, i.e., Li-Ion batteries, become a more cost-effective way of meeting the night-time electricity demands of the plant than using grid-sourced electricity. We attribute the suddenness of the step change, as opposed to a gradual transition, as being due to the change in battery cycle lifetime resulting in a change in the number of battery replacements that are required throughout the lifetime of the system. As degradation rate of the batteries depends on the amount of electricity which is passed through them, there is no correlated gradual change as was observed when changing the inverter cycle lifetime in Figure 1.

# 4 Component selection results

The effect of changing the specific collector model used for the PV, PV-T and solar-thermal collectors was explored, with the specific collector which resulted in the overall lowest costs over the lifetime of the plant given in Table 3. The data show that, across all four case-study locations, systems which utilised the p-Si panel selected were associated with a lower total cost over the lifetime of the plant compared with those utilising the m-Si panel selected.

For the medium- and largest-scale plants, the results in Table 3, also visible in the main text, demonstrate that the relatively low-thermal-efficiency, lower-cost STI FPC and Eurotherm ETC are associated with the lowest-cost systems. This is in constrast to the results for the smallest-scale plant, where the relatively high-cost and high-thermal-efficiency Augusta ETC is utilised to produce cheaper systems. We attribute this difference to the lower auxiliary-heating fraction for the lowest-capacity plant of 15.2% resulting in a greater reliance on the performance of S-T and PV-T collectors installed compared with the higher auxiliary-heating fractions of 80.1% and 37.0% for the medium- and largest-scale desalination plants respectively, where S-T and PV-T collectors provide less thermally-driven heating and thus the lower-performance and -cost collectors are associated with systems with the lowest lifetime cost.

The dependence of the lowest lifetime cost system on the PV-T panel chosen is not strongly correlated with the cost of grid-sourced electricity, as shown in Table 3. For Gando in Gran Canaria, and Tijuana and La Paz in Mexico, systems that employed DualSun 300 collectors were associated with overall lower lifetime costs than those which employed either DualSun 400 or Solimpeks Powervolt collectors. This is potentially due to the balance between a high reference electrical efficiency and thermal efficiency of the DualSun 300 collectors at a comparatively low cost of 556$ per collector with a reference efficiency of 18.3% compared with 1022 $ and 21.3% and 545$ and 15.08% for the DualSun 400 and Solimpeks Powervolt collectors respectively, enabling them to be a competitive way to provide day-time electricity and heat synergistically to the MED plant for these relatively smaller systems. However, with the lowest-cost system for Abu Dhabi and Gran Canaria for the smallest-capacity plant consisting of 1 and 0 PV-T collectors respectively, it is likely that the choice of PV-T technology is not significant compared with the choice of technology for the other components or for the larger-capacity plants.

For Tijuana and La Paz, the greater reliance of the system on PV-T and S-T collectors for hot-water heating as opposed to electrically-powered auxiliary heating is visible in the greater combined number of S-T and PV-T collectors installed on average, the results of which are given in Table **??**. This greater dependence on solar-thermally-driven heating is potentially responsible for the shift to the cheaper and less electrically-efficient Powervolt collector being associated, on average, with systems that have a lower total lifetime cost.

# 5 Emissions-cost comparison results

A scatter plot, along with an overlaid kernel-density estimate for the same data, plotted for clarity, of the specific emissions and costs across all technology combinations is shown in Figure 3. The KDE envelope has been clipped just beyond the bounds of the data to prevent a misleading envelope highlighting regions where there is no data as a result of the fit.

The results in Figure 3 echo the results from the main paper, namely that the energy-generation system for MED desalination is cheaper than grid-powered RO in Tijuana and La Paz in Mexico and more expensive in Abu Dhabi in the UAE and Gando in Gran Canaria due to the comparatively low price of grid-sourced electricity in the UAE and on Gran Canaria. Here, in Figure 3, the data show that this is the case irrespective of the technology combination that results in the lowest-cost system, with all results fitting between the specific costs associated with grid-powered RO in Abu Dhabi and Gando, and Tijuana and La Paz. The data also reiterate the results from Figure **??**, namely that MED desalination in Abu Dhabi, Tijuana and La Paz can produce as few emissions as the energy associated with grid-powered RO in these locations.

Figure 3 also shows that systems installed in La Paz were associated with the lowest specific emissions of any of the four-case study locations. La Paz has the highest cost of grid electricity of the four case-study locations considered which results in none of the technology combinations shown in Figure 3 for La Paz utilising grid-sourced electricity. Across the four case-study locations (Abu Dhabi, Gando, Tijuana and La Paz), the lowest-cost systems plotted have mean grid electricity fractions of 45.0%, 0.00778%, 0.00% and 0.00%. Hence, differences in the specific emissions visible in Figure 3 for Tijuana and La Paz are due to different system capacities being needed to meet fulfil the demands of the plant across technology combinations rather than variations in the auxiliary-heating and grid-electricity fractions. The reduced spread in the auxiliary-heating fraction in Tijuana as opposed to La Paz, 0.666% and 6.03% respectively, and the reduced spread of the number of components installed results in the reduced spread of the data with a greater number of results for Tijuana being concentrated in Figure 3.

Systems in Gando, shown in yellow in Figure 3, generally have higher associated costs and emissions than Abu Dhabi, shown in red. Due to the non-zero grid electricity fractions in both Abu Dhabi and Gran Canaria across the systems plotted, this can be partly attributed to the emissions associated with

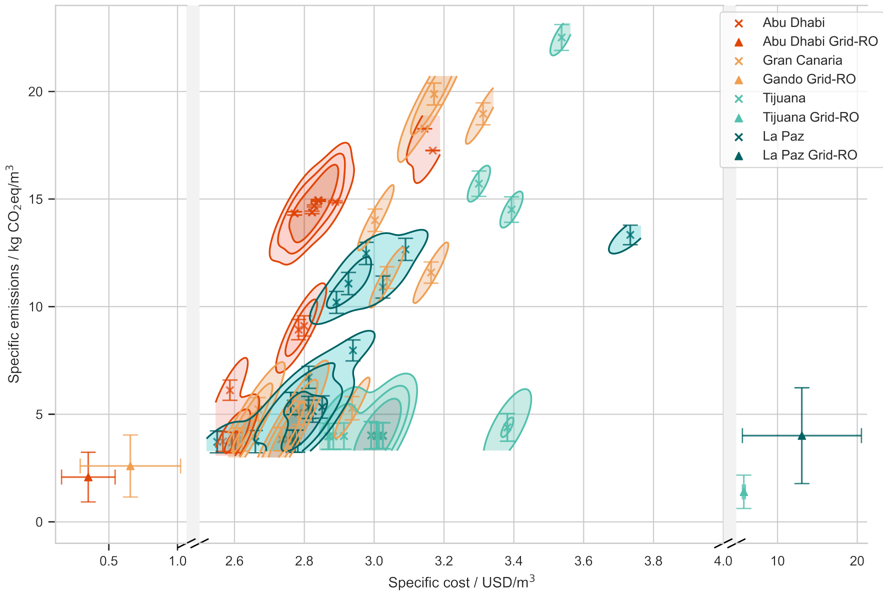


**Fig. 3 Cost-emissions scatter for all component combinations.** Scatter plot with an overlaid kernel-density estimate of the specific emissions against specific costs of the energy-generation system for MED desalination. Each point corresponds to a specific combination of energy-generation technologies, detailed in Tables **??**, **??** and **??**, where the system has been optimised for the lowest total lifetime cost. The specific emissions and costs associated with the grid electricity consumed in grid-powered RO are also shown. The data show that optimising for the lowest lifetime cost can produce systems which range in cost and emissions intensity depending on the choice of technology as demonstrated in Figure **??**. The data show that locations with a relatively low cost of grid-sourced electricity, i.e., Abu Dhabi and Gando with specific grid costs of 0.078 $/kWh$_{el}$ and 0.146 $/kWh$_{el}$ respectively, are associated with a lower specific cost for a fixed specific-emissions value. The results also show that La Paz, despite having the highest emissions intensity of grid electricity at 890 g $CO_2$eq/kWh$_{el}$, is associated with lower specific emissions than Abu Dhabi, Gando and Tijuana. The data reiterate the findings displayed in Figures **??** and **??**, namely that grid-powered RO is cheaper than MED desalination in Abu Dhabi and Gando and more expensive elsewhere, and that the specific emissions resulting from MED-driven desalination are comparable to grid-powered RO in all locations other than Tijuana.

electricity drawn from the grid. For Gando, the relatively low grid electricity fraction, 0.00778% on average and up to 0.0691%, implies that a large part of the variation in the emissions shown in Figure 3 is a result of changing technology choice rather than a variance in the reliance of the system on grid-sourced electricity and thus variations in the resulting emissions.

Overall, the data in Figure 3 show that, whilst PV-, PV-T- and S-T-driven MED desalination can produce clean water with specific costs lower than grid-driven RO (as is visible for Tijuana and La Paz), and with emissions that are comprable within error to grid-driven RO for all locations other than Tijuana, the choice of specific collector used can have a significant impact. The spread of points demonstrates variations in cost by a factor of 1.5 and in emissions by a factor of around 8 depending on the collector model utilised. It is therefore key when considering whether MED desalination is suitable, and what capacity of collectors are needed to meet the demands of the plant, the specific location and technologies which are available as this choice can have a great impact on overall lifetime costs and emissions.

# References

[1] Quansah, D. A., Adaramola, M. S. & Takyi, G. Degradation and longevity of solar photovoltaic modules—an analysis of recent field studies in ghana. *Energy Sci. Eng.* **8** (6), 2116–2128 (2020). URL https://onlinelibrary.wiley.com/doi/10.1002/ese3.651. https://doi.org/10.1002/ese3.651 .

[2] Edge, J. S. *et al.* Lithium ion battery degradation: what you need to know. *Phys. Chem. Chem. Phys.* **23** (14), 8200–8221 (2021). URL http://dx.doi.org/10.1039/d1cp00359c. https://doi.org/10.1039/d1cp00359c .

[3] Spotnitz, R. Simulation of capacity fade in lithium-ion batteries. *Journal of Power Sources* **113** (1), 72–80 (2003). URL https://www.sciencedirect.com/science/article/pii/S0378775302004901. https://doi.org/10.1016/S0378-7753(02)00490-1 .

[4] United Nations General Assembly. Transforming our world: the 2030 agenda for sustainable development, 21 October 2015, A/RES/70/1. https://www.refworld.org/docid/57b6e3e44.html (2015). URL https://www.refworld.org/docid/57b6e3e44.html. Accessed: 2021-6-15.

[5] Gao, C. *et al.* Comprehensive comparison of multiple renewable power generation methods: A combination analysis of life cycle assessment and ecological footprint. *Renewable Sustainable Energy Rev.* **147**, 111255 (2021). URL https://www.sciencedirect.com/science/article/pii/S1364032121005426. https://doi.org/10.1016/j.rser.2021.111255 .

[6] Cucchiella, F. & D'Adamo, I. Estimation of the energetic and environmental impacts of a roof-mounted building-integrated photovoltaic systems. *Renewable Sustainable Energy Rev.* **16** (7), 5245–5259 (2012). URL https://www.sciencedirect.com/science/article/pii/S1364032112003097. https://doi.org/10.1016/j.rser.2012.04.034 .

[7] Todde, G. *et al.* Embodied energy and environmental impact of Large-Power Stand-Alone photovoltaic irrigation systems. *Energies* **11** (8), 2110 (2018). URL https://www.mdpi.com/1996-1073/11/8/2110. https://doi.org/10.3390/en11082110 .

[8] Liu, J., Chen, S., Wang, H. & Chen, X. Calculation of carbon footprints for water diversion and desalination projects. *Energy Procedia* **75**,

2483–2494 (2015). URL https://www.sciencedirect.com/science/article/pii/S1876610215010073. https://doi.org/10.1016/j.egypro.2015.07.239 .

[9] Alhaj, M., Tahir, F. & Al-Ghamdi, S. G. Life-cycle environmental assessment of solar-driven Multi-Effect desalination (MED) plant. *Desalination* **524**, 115451 (2022). URL https://www.sciencedirect.com/science/article/pii/S0011916421005221. https://doi.org/10.1016/j.desal.2021.115451 .

[10] Michael, J. J. & Selvarasan, I. Economic analysis and environmental impact of flat plate roof mounted solar energy systems. *Solar Energy* **142**, 159–170 (2017). URL https://www.sciencedirect.com/science/article/pii/S0038092X16306132. https://doi.org/10.1016/j.solener.2016.12.019 .

[11] Henein, S. M., Abdel-Rehim, A. A. & El-Nagar, K. Energy, economic and environmental analysis of an evacuated tube solar collector using hybrid nanofluid. *Appl. Therm. Eng.* **219**, 119671 (2023). URL https://www.sciencedirect.com/science/article/pii/S1359431122016015. https://doi.org/10.1016/j.applthermaleng.2022.119671 .

[12] Lu, J. *et al.* Spatiotemporal analysis of the future carbon footprint of solar electricity in the united states by a dynamic life cycle assessment. *iScience* **26** (3), 106188 (2023). URL http://dx.doi.org/10.1016/j.isci.2023.106188. https://doi.org/10.1016/j.isci.2023.106188 .

[13] Moret, S. *Strategic energy planning under uncertainty.* Ph.D. thesis, EPFL (2017). URL http://infoscience.epfl.ch/record/231814.

[14] Philippot, M., Alvarez, G., Ayerbe, E., Van Mierlo, J. & Messagie, M. Eco-Efficiency of a Lithium-Ion battery for electric vehicles: Influence of manufacturing country and commodity prices on GHG emissions and costs. *Batteries* **5** (1), 23 (2019). URL https://www.mdpi.com/2313-0105/5/1/23. https://doi.org/10.3390/batteries5010023 .

[15] The Chartered Institution of Building Services Engineers (CIBSE). Embodied carbon in building services: A calculation methodology (TM65). Tech. Rep. (2014).

[16] Grant. Grant MonoWave system indirect HP (heat pump) cylinder. https://www.grantuk.com/media/3775/monowave-indirect-heat-pump-cylinder-installer-and-user-uk-doc-0134-rev-1-1-october-2020.pdf (2020). URL https://www.grantuk.com/media/3775/monowave-indirect-heat-pump-cylinder-installer-and-user-uk-doc-0134-rev-1-1-october-2020.pdf. Accessed: 2023-3-14.

[17] Tschümperlin, L., Stolz, P., Wyss, F. & Frischknecht, R. Life cycle assessment of low pow- er solar inverters (2.5 to 20 kw).

Tech. Rep., {Swiss Federal Office of Energy (SFOE)} (2016). URL https://treeze.ch/fileadmin/user_upload/downloads/Publications/Case_Studies/Energy/174-Update_Inverter_IEA_PVPS_v1.1.pdf.

[18] Constantino, G., Freitas, M., Fidelis, N. & Pereira, M. G. Adoption of photovoltaic systems along a sure path: A Life-Cycle assessment (LCA) study applied to the analysis of GHG emission impacts. *Energies* **11** (10), 2806 (2018). URL https://www.mdpi.com/1996-1073/11/10/2806. https://doi.org/10.3390/en11102806 .

[19] Hodencq, S., Coignard, J., Kofi, T.-D. N. & Hajiro, N. M. L. Including greenhouse gas emissions and behavioural responses in the optimal design of PV self-sufficient energy communities. *COMPEL - The international journal for computation and mathematics in electrical and electronic engineering* **41** (6), 2072–2083 (2022). URL https://doi.org/10.1108/COMPEL-10-2021-0392. https://doi.org/10.1108/COMPEL-10-2021-0392 .

[20] Buira, D. *et al.* A whole-economy deep decarbonization pathway for mexico. *Energy Strategy Reviews* **33**, 100578 (2021). URL https://www.sciencedirect.com/science/article/pii/S2211467X20301310. https://doi.org/10.1016/j.esr.2020.100578 .

[21] Winchester, B., Nelson, J. & Markides, C. N. HEATDesalination (2023). URL https://zenodo.org/record/7612966.

[22] Ritchie, H., Roser, M. & Rosado, P. Energy. *Our World in Data* (2022) .

[23] Barone, G., Buonomano, A., Forzano, C., Giuzio, G. F. & Palombo, A. Supporting the sustainable energy transition in the canary islands: Simulation and optimization of multiple energy system layouts and economic scenarios. *Frontiers in Sustainable Cities* **3** (2021). URL https://www.frontiersin.org/articles/10.3389/frsc.2021.685525. https://doi.org/10.3389/frsc.2021.685525 .

[24] Center for Climate Strategies (CCS). Final report of the baja california phase 2 climate action plan. Tech. Rep. (2014). URL https://uccrnna.org/wp-content/uploads/2017/06/2014_Baja-California_Climate-Action-Plan.pdf.

[25] Ivanova, A., Bermudez, A. & Martinez, A. in *Climate action plan for the city of la paz, baja california sur, mexico: A tool for sustainability* , Vol. 194 439–449 (WIT Press, 2015). URL http://www.witpress.com/elibrary/wit-transactions-on-ecology-and-the-environment/194/34380.

[26] Ritchie, H. & Roser, M. CO2 and greenhouse gas emissions. *Our World in Data* (2020). URL https://ourworldindata.org/

co2-emissions?utm_source=squamish%20chief&utm_campaign=squamish%20chief&utm_medium=referral .

[27] Ember. Yearly electricity data. https://ember-climate.org/data-catalogue/yearly-electricity-data/ (2022). URL https://ember-climate.org/data-catalogue/yearly-electricity-data/. Accessed: 2023-3-6.

[28] Qiblawey, Y., Alassi, A., Zain ul Abideen, M. & Bañales, S. Techno-economic assessment of increasing the renewable energy supply in the canary islands: The case of tenerife and gran canaria. *Energy Policy* **162**, 112791 (2022). URL https://www.sciencedirect.com/science/article/pii/S0301421522000167. https://doi.org/10.1016/j.enpol.2022.112791 .

[29] Ritchie, H., Roser, M. & Rosado, P. CO2 and greenhouse gas emissions. *Our World in Data* URL https://ourworldindata.org/co2-and-greenhouse-gas-emissions .

[30] Yang, X.-G., Zhang, G., Ge, S. & Wang, C.-Y. Fast charging of lithium-ion batteries at all temperatures. *Proc. Natl. Acad. Sci. U. S. A.* **115** (28), 7266–7271 (2018). URL http://dx.doi.org/10.1073/pnas.1807115115. https://doi.org/10.1073/pnas.1807115115 .

[31] Rohr, S. *et al.* Quantifying uncertainties in reusing Lithium-Ion batteries from electric vehicles. *Procedia Manufacturing* **8**, 603–610 (2017). URL https://www.sciencedirect.com/science/article/pii/S2351978917300835. https://doi.org/10.1016/j.promfg.2017.02.077 .

[32] Peng, X., Chen, S., Garg, A., Bao, N. & Panda, B. A review of the estimation and heating methods for lithium-ion batteries pack at the cold environment. *Energy Sci. Eng.* **7** (3), 645–662 (2019). URL https://onlinelibrary.wiley.com/doi/10.1002/ese3.279. https://doi.org/10.1002/ese3.279 .

[33] Sangwongwanich, A., Yang, Y., Sera, D. & Blaabjerg, F. Lifetime evaluation of Grid-Connected PV inverters considering panel degradation rates and installation sites. *IEEE Trans. Power Electron.* **PP** (99), 1–10 (2017). URL https://www.researchgate.net/publication/314121765_Lifetime_Evaluation_of_Grid-Connected_PV_Inverters_Considering_Panel_Degradation_Rates_and_Installation_Sites. https://doi.org/10.1109/TPEL.2017.2678169 .

[34] Joo, H.-J. & Kwak, H.-Y. Performance evaluation of multi-effect distiller for optimized solar thermal desalination. *Applied Thermal Engineering* **61** (2), 491–499 (2013). URL https://www.sciencedirect.com/science/article/pii/S1359431113005644. https://doi.org/10.1016/j.applthermaleng.2013.08.006 .

[35] El-Nashar, A. M. & Samad, M. The solar desalination plant in abu dhabi: 13 years of performance and operation history. *Renewable Energy* **14** (1), 263–274 (1998). URL https://www.sciencedirect.com/science/article/pii/S0960148198000767. https://doi.org/10.1016/S0960-1481(98)00076-7 .

[36] Rahimi, B., May, J., Christ, A., Regenauer-Lieb, K. & Chua, H. T. Thermo-economic analysis of two novel low grade sensible heat driven desalination processes. *Desalination* **365**, 316–328 (2015). URL https://www.sciencedirect.com/science/article/pii/S0011916415001599. https://doi.org/10.1016/j.desal.2015.03.008 .

**Table 3** Technology choice and specific cost of the energy-generation system for the combination of collectors associated with the lowest-cost system across the plant capacities and case-study locations

| Plant | $\dot{m}_{\text{prod}}$, $m^3$/day | Location | PV type | PV-T type | S-T type | Specific cost, $\$/m^3$ |
|---|---|---|---|---|---|---|
| Small | 3 [34] | Abu Dhabi | REC | Solimpeks | Augusta | 6.37 |
| | | Gran Canaria | Sharp | D.S. 300 | Augusta | 6.40 |
| | | Tijuana | Sharp | D.S. 300 | Augusta | 6.94 |
| | | La Paz | Sharp | D.S. 300 | Augusta | 6.49 |
| Medium | 120 [35] | Abu Dhabi | REC | D.S. 300 | Augusta | 2.57 |
| | | Gran Canaria | Sharp | D.S. 400 | Augusta | 2.61 |
| | | Tijuana | Sharp | D.S. 300 | Eurotherm | 2.87 |
| | | La Paz | Sharp | Solimpeks | STI | 2.55 |
| Large | 1694 [36] | Abu Dhabi | Sharp | D.S. 300 | Eurotherm | 2.74 |
| | | Gran Canaria | Sharp | Solimpeks | Augusta | 2.93 |
| | | Tijuana | Sharp | D.S. 400 | STI | 3.21 |
| | | La Paz | REC | Solimpeks | STI | 3.05 |